Appl. Chem. Eng., Vol. 27, No. 5, October 2016, 483-489
http://dx.doi.org/10.14478/ace.2016.1066

Article

용이한 마이크로웨이브 조사법을 사용하여 합성한 이원계 Cu (I) 셀렌 그래핀 나노복합체의 광촉매 염료분해 효과

아즈가 알리 · 오원춘†

한서대학교 신소재공학과
(2016년 7월 7일 접수, 2016년 7월 28일 심사, 2016년 8월 5일 채택)

Photocatalytic Dye Decomposition Effect of Binary Copper (I) Selenide-graphene Nanocomposites Synthesized with Facile Microwave-assisted Technique

Asghar Ali and Won-Chun Oh†

Department of Advanced Materials Science & Engineering, Hanseo University, Seosan 31962, Korea
(Received July 7, 2016; Revised July 28, 2016; Accepted August 5, 2016)

초 록

본 연구에서 쉽고 빠른 마이크로 조사법을 사용하여 합성한 Cu_2Se-그래핀 나노복합체를 광촉매 분해 효과를 연구하였다. 제조된 나노복합체는 XRD, SEM, TEM, 라만분광분석, XPS 및 UV-Vis 흡수분광법을 사용하여 특성화하였다. 그리고 광촉매 분해특성을 가시광선 조사하에 표준염료인 로다민 B의 분해를 통하여 연구하였다. Cu_2Se-그래핀 복합체는 상당히 우수한 광촉매 분해 효과를 나타내었고, 이는 180 min 동안 가시광선 조사하에서 약 95%의 분해 효과를 나타내고 있음을 이들 결과로부터 알 수 있었다. 결론적으로 Cu_2Se-그래핀 복합체는 염료 오염물질에 대한 적합한 촉매로 사용할 수 있음을 확인하였다.

Abstract

Here, we examined the photo-degradation efficiency of Cu_2Se-graphene nanocomposites synthesized by a facile and fast microwave-assisted technique. The prepared composites were characterized by X-ray diffraction (XRD), scanning electron microscopy (SEM), transmission electron microscopy (TEM), Raman spectroscopy, XPS and UV-Vis spectrophotometry. The photocatalytic performance was studied through the decomposition of Rhodamine (Rh B) as a standard dye under visible light radiation. A 95% of Rh B degradation after visible light irradiation for 180 min indicates that the Cu_2Se-graphene composite exhibited significant photodegradation efficiency. Therefore, it can be concluded that the synthesized Cu_2Se-graphene can be used as a suitable catalyst for decomposing dye pollutants.

Keywords: *graphene, semiconductor, photocatalysts, XRD, TEM, raman, photo-degradation*

1. Introduction

Recently, dyes are the most prominent toxin in aquatic environments because of their enormous volume of production from industries, slow biodegradation character, low decoration character and toxicity[1]. During the last decades a chain of experiments have been attempted all over the world to find proper materials to degrade toxic pollutants. Synthetic dyes are largely used in commercial industries. Thousands of different types of commercial dyes and pigments are produced million tons annually. During the dyeing process, approximately 10-15% of the dyes are released into the environment that plays a key role in water pollution[2]. Many techniques used for the removal of dyes form wastewater, such as membrane filtration[3], absorption[4], elerocoagulation[5], ozonation[6], Fenton oxidation[7], ion flotation[8], sonocatalytic degradation[9], and photocatalytic degradation[10,11]. Among those techniques, photocatalytic degradation has been found to be favorable process for dye wastewater treatment due to these technique easily covert harmful organic contaminants into carbonaceous products[12]. Therefore a worldwide researchers have been focuses the degradation techniques of dye pollutants for a long time. Several catalysts have been used for photocatalytic degradation of dyes such as Ag-Au-ZnO[13], polyethylene-TiO_2[14], Bi_2WO_6[15], (Yb, N)-TiO_2[16], hollow cobalt (Co) nanoparticles[17], Si/Si_x core-shell nanowires[18], SnS Nanorods[19], biogenic silver nanoparticles (AgNPs)[20], Ni nanoparticles decorated SiO_2/TiO_2 magnetic spheres (Ni-SiO_2/TiO_2)[21] and carbon-modified antimony sulfide (Sb_2S_3)[21]. But these catalysts have some drawbacks

† Corresponding Author: Hanseo University,
Department of Advanced Materials Science & Engineering, Seosan 31962, Korea
Tel: +82-41-660-1337 e-mail: wc_oh@hanseo.ac.kr

pISSN: 1225-0112 eISSN: 2288-4505

in either limiting by its UV activation requirement or complexity of preparation process, therefore new catalysts have recently been developed. In present time, Cu_2Se used is a promising photocatalyst and it has been vastly used for photocatalytic degradation of pollutant, due to its unique properties and wide applications in solar cell, gas sensors, thermoelectric converts etc. direct band gap of the Cu_2Se in the range of 1.9-2.3 eV and indirect band gap in the range 1.2-1.7 eV[22]. Among these, $Cu_{2-x}Se$ nanocrystals show efficient photocatalytic activity (50% with irradiation time of 2 h) towards the photodegradation of RhB aqueous solution under visible light due to its suitable band gap[23]. Apart from this, recently graphene plays a vital role in the photocatalysis filed, graphene-based materials have has been widely studied due to excellent properties (e.g. high thermal conductivity ≈ 5000 $Wm^{-1}k^{-1}$ and highly surface area ≈ 2600 m^2g^{-1}). These remarkable properties increase the charge transfer separation of the electron and holes[24,25]. These photogenerated holes and electron play an important role in pollutant degradation and photocatalytic redemption.

Furthermore Microwave irradiation techniques are very effective in the fast and facial route for preparation of binary or ternary compound, MW-assisted techniques are low consumption of energy, and a low production cost and successfully decreasing the reaction time up to a few minutes and also suppresses side reactions, with high phase purity and high yield[26,30]. There is no doubt that the microwave technique has the potential to fulfill all areas of synthetic chemistry. Especially, the synthesis of nanoparticles and nanostructures, nanostructured, carbonmaterials, nanoporous nanomaterials, metal oxide nanoparticles supported on carbon nanotubes, and polymer nanocomposites[31,35].

Here, we reported Cu_2Se nanoparticles were attached onto the graphene through microwave-assisted techniques.In this procedure, GO is merged with copper (ii) and Se precursor materials under proper condition. During microwave irritation, graphene oxide converts to graphene and attachment of Cu_2Se nanoparticles on the graphene sheets was observed in ethylene glycol. The photocatalytic activities were tested with Rh. B as a standard dye under UV/Vis light.

2. Experimental

2.1. Materials

Copper (ii) nitrate trihydrate ($Cu(NO_3)_2・3H_2O$), selenium powder (Se, 99%), ammonium hydroxide (NH_4OH, 25-28%), Sodium sulfite ($Na_2SO_3・7H_2O$, 95%), and ethyl alcohol (94%) were purchased from Duksan Pure Chemical Co. Ltd., Korea. Rhodamine B(RhB) was used as an industrial organic pollutant, purchased from Texchem Korea Co. Ltd. All chemicals were used without further purification. All dilutions were carried out using distilled water.

2.2. Preparation of graphene

Graphene oxide was prepared in the laboratory following the Hummer's-Offeman method as highlighted in different articles[36-38]. In brief, 20 g natural graphite and H_2SO_4 (400 mL) were homogeneously mixed at 0 ℃ with constant magnetic stirring. Then, 40 g of $KMnO_4$ slowly mixed to the above solution and the temperature was kept below 14 ℃. The resulting mixture was continuously stirred at 35 ℃ until it became dim brownish. And then diluted to 150 mL using De-ionized (DI) water and kept stirring at below 90 ℃. After adding De-ionized (DI) water, the container was sealed and kept at 100 ℃ with vigorous stirring for 30 min, meanwhile 20% H_2O_2 added drop wise within 5 min and then the solution was washed with acetone and 10% HCl several time to remove residual metal ions. The solution was then heat-treated in the dry oven at 90 ℃ for 12 h to obtain graphite oxide power, then take 250 mg graphite oxide power were added to 200 mL DI water vigorously stirred for 30 min and then ultrasonicated (using Ultrasonic Processor, VCX 750) for 2 h. Finally the resulting solution were refined and washed several times with hot water and kept in a dry oven for 6 h to obtain graphene oxide power.

2.3. Preparation of copper selenide composite

In a typical synthesis process, 1.5 g of anhydrous sodium sulfite (Na_2SO_3) and 0.3 g crude selenium (Se) power were dispersed in 200 mL of ethylene glycol continuously stirring until homogenous mixture(selenium salt) was obtained. In next step 0.675 g of copper (ii) nitratetrihydrate $Cu(NO_3)_2・3H_2O$ was mixed to selenium salt solution and stirred for 30 min obtain a stable solution. Finally solution was transferred to a 500 mL reaction vessel placed in a conventional microwave for 500 s, with 10 sec on and 10 sec off state. The Cu_2Se precipitates was then cooled to room temperature and filtered with using 47 mm Whatman filter paper, and heated at a temperature of 350 K for 10 h to obtain a Cu_2Se power.

2.4. Preparation of Cu_2Se-graphene nanocomposite

Cu_2Se-graphene nanocomposite was obtained by following above method. A borosilicate glass sealed reaction vessel specially designed for microwave techniques. Graphene oxide (200 mg) was added in 100 mL ethylene glycol and then exfoliated to generate graphene oxide nanosheets (GONS) dispersion solution by ultrasonication for 30 min and then 0.675 g of copper (ii) nitratetrihydrate $Cu(NO_3)_2・3H_2O$ were dispersed in 100 mL ethanol and water mixed in equal volumetric ratios of 1 : 1 by ultrasonication for 1 h using a digital sonifer to obtain graphene oxide nanosheets (GONS)/Cu^{+2} solution. In addition selenium powder and 6 mL NH_4OH (28 wt%) were added to the solution, the mixture was vigorously stirred for 30 min, then the solution irradiated by microwave, and solution irradiated by microwave at full power for 10 sec on and 10 sec off (for total 500 s), and cooled at room temperature washed several time with hot water and transferred into a dry oven. The weight ratios of graphene oxides to Cu_2Se were taken 1, 2 and 3.5% and then obtained were labeled Cu_2Se-graphene 1, Cu_2Se-graphene 2 and Cu_2Se-graphene 3 respectively.

2.5. Photocatalytic degradation experiment of Rhodamine B(RhB)

The adsorption and photocatalytic performance of the as-prepared Cu_2Se-graphene was evaluated by the degradation of Rh.B dye under visible light. A xenon (8 W, λ > 420 nm) used as a visible light source. In the experiment, 20 mg of the Cu_2Se-graphene catalytic sam-

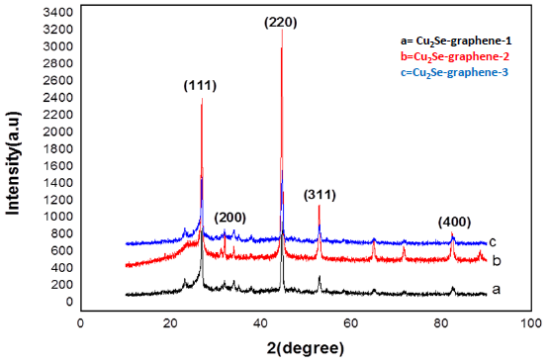

Figure 1. X-ray diffraction (XRD) patterns of Cu_2Se-graphene composites.

ple was dispersed 100 mL solution of Rh.B (2.0×10^{-6} mol/L). In order to reach adsorption-desorption equilibrium, the solution was kept in dark for 2 h. Before switched on the light source, a sample was collected from the solution and kept in a centrifuge at 10,000 rpm for the elimination of solid materials. After that, the light source was tune on and samples were collected in every 30 min and then the samples were centrifuged for 10 min to remove any suspended solid. All the samples were irradiated for 180 min to compare their catalytic efficiencies.

2.6. Characterization of catalysts

For measurements of crystallinity of the prepared samples, XRD patterns were taken using monochromatic high intensity Cu Kα radiation (λ = 1.5406 Å) in XRD (Shimadzu XD-D1). The surface area and morphology of the prepared simple were observed using SEM (JS M-5600 JEOL, Japan). For further detailed study of the composite particles was determined by TEM (JE OL, JEM- 2010, and Japan). The change in absorbance was measured using UV-Vis spectrophotometer (Optizen POP, Korea). Raman spectra of the prepared samples were observed using a spectrometer (Jasco Model Name NRS-3100) with an excitation laser wavelength of 532.06 nm. The photocatalytic performance of the Cu_2Se-graphene was investigated by absorbance spectrometry whit a UV/Vis spectrophotometer (Optizen POP, Mecasys, Korea).

3. Results and Discussion

The crystal structure and composition of Cu_2Se-graphene via microwave-assisted techniques were analyzed by power XRD measurement. The Figure 1 illustrates that these three kinds of nanocomposites have a similar diffraction patterns that correspond to a monoclinic crystal phase (JCPDS PDF#00-06-0680). The XRD diffraction peaks of the Cu2Se-graphene compound present around 2θ of 26.7, 44.5, 52.6 and 65.7°, which can be indexed to the characteristic peak (111), (220), (311), and (400) plane reflections[39,40]. From Figure 1, it can be seen that the diffractogram of graphene exhibits the typical peaks at 26.7°, which corresponds to the (002) hexagonal planes of crystalline graphite. The intensity of the peaks is very small compared to the Cu_2Se peaks. The suppressing of the different peaks verifies the minimal development of crystalline phases on the graphene sheets. The intensity fluctuation of the diffraction peaks for the nanocomposites also justifies the increased amount of graphene and suppression of the crystalline phases. The peak intensity decreasing also confirms that the lattice structure of Cu_2Se is distorted by the interaction with graphene oxides[41,42]. Morphologies of Cu_2Se, graphene and Cu_2Se-graphene nanocomposites were examined by SEM. Figure 2 (a-c) predicted the overall structure of the nanocomposites. And, it can be clearly indicated that graphene is plate like structure broken off in different direction and Cu_2Se nanoparticles are corporate into group of clusters (Figure 2 (a)). The Figure 2 (b) illustrates an irregular structure of graphene and bright spots indicated a pure Cu_2Se particles appear as spherical particles and unevenly distributed. Moreover Cu_2Se-graphene nanocrystals were partially agglomerated and formed the bunch of clusters around the graphene sheet formed a graphene-based nanostructure composite (Figure 2 (c)). Furthermore, the plate-like structures presented the presence of oxygen containing functional groups on the surface of the graphene sheets[43]. The information of the microscopic structure for the Cu_2Se-graphene composite was examined by TEM technique with different magnification as shown in Figure 3.

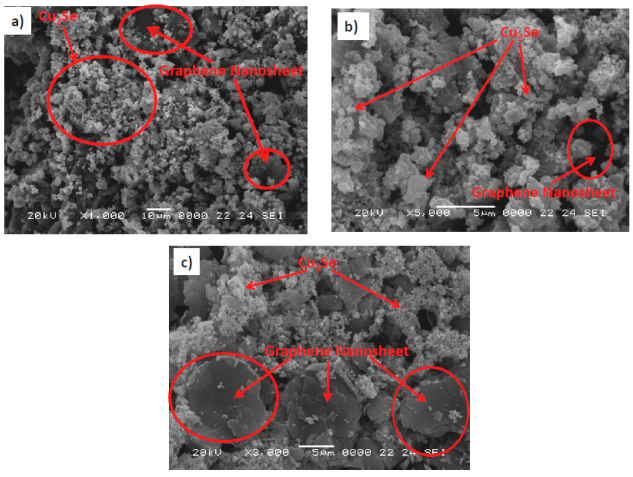

Figure 2. SEM images of Cu_2Se-graphene composites with different magnification.

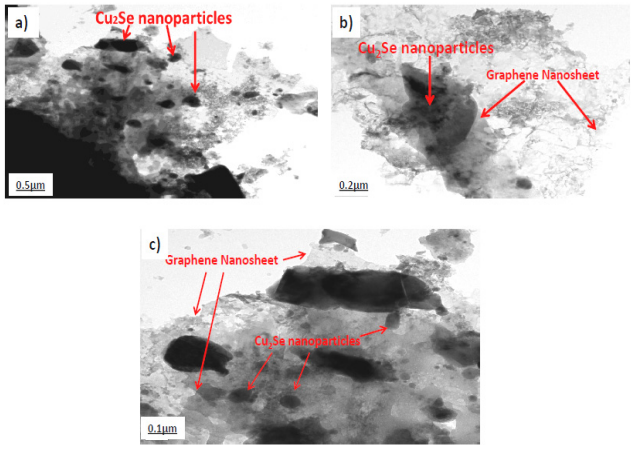

Figure 3. TEM images of Cu_2Se-graphene composites with different magnification.

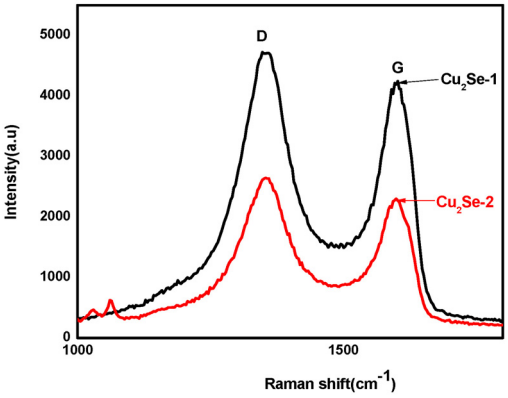

Figure 4. Raman spectra of Cu_2Se-graphene nanocomposites.

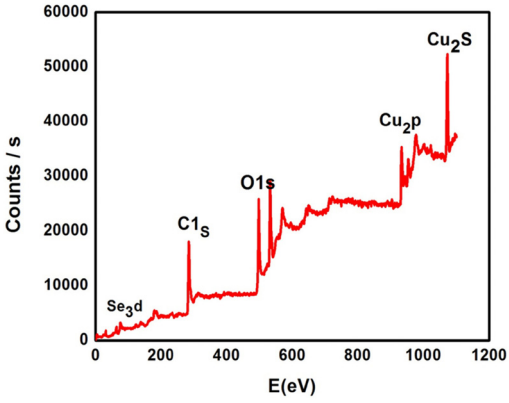

Figure 5. XPS survey scan spectrum of Cu_2Se-graphene nanocomposites.

From Figure 3 (a-b), it revealed that the two dimensional structure of graphene sheet with few layers was retained after microwave assisted hydrothermal treatment, and also observed that average size of the nanoparticles are approximately 0.3 to 0.5 μm (using image J software). Figure 3 (c) suggests that the graphene sheets are well distributed and providing a large microsheet type plate structure to Cu_2Se nanoparticles. Furthermore, the Figure 3 (c) also subscribes the interactions between graphene sheet and Cu_2Se nanospheres, which may give increase electrocatalytic performance[44]. The Figure 4 shows Raman spectra which provide further information about the nature and quality of the graphene (e.g. number of layers and the crystal structure). The Raman spectra of Cu_2Se-graphene nanocomposites displayed D band at 1353 cm^{-1} and a sharp G band at 1588 cm^{-1}. These two peaks labeled G-band and D-band gives information on the nature of carbon-carbon bonds and defects[45,46]. The D band corresponds to the vibration of the carbon atom in disordered or defect sites, which is an ordinary feature of sp^3 defects. While the G band peak can be attributed to sp^2-bonded carbon atoms[47]. The intensity ratio of D band and G band (I_D/I_G) generally indicates the degree of reduction of GO to graphene. The $I_D/I_G \approx 1.2$ indicated that the increase in the number of graphene layers[48].

X-ray photoelectron spectroscopy (XPS) analysis was used for the chemical composition and bonding configuration of the prepared nanocomposites. Figure 5 depicted the full survey spectrum indicated

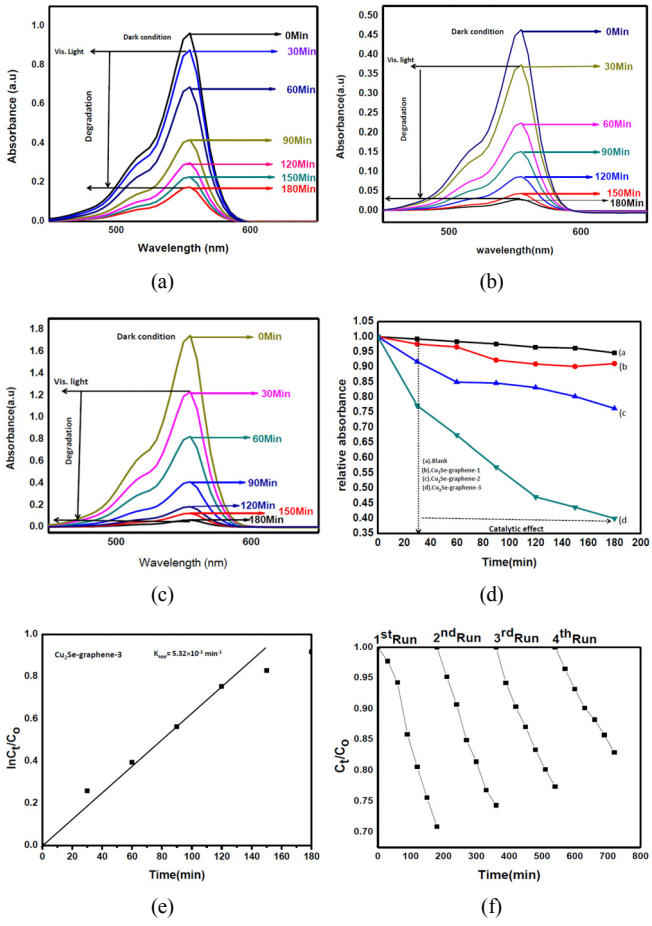

Figure 6. UV-vis diffuse reflectance spectra of copper (I) selenide-graphene nancomposites; (a) Cu_2Se-ghaphene-1, (b) Cu_2Se-graphene-2, (c) Cu_2Se-graphen-3 (d) Rh.B degradation efficiency with respect to time, (e) Kinetics of degradation of Cu_2Se-graphene-3 composite under visible light irradiation and (f) Cycling run in the photodegradation of Rh.B in the Cu_2Se-graphene-3.

peaks corresponding to all components exhibited the formation of Cu_2Se-graphene nanocomposites. From the figure clearly shown that the selenium 3d core level two peaks placed at 54.60 eV and 58.9 eV, which indicated that the lattice Se-2 and an oxidation state of Se[49], and O1s (530 eV) presented C=O and O-C-OH groups[50,51]. The position C 1s (284.5eV) peak has shown the characteristic sp2 carbon corresponding to C-C groups[52]. The main peak of the Cu2p core level corresponding at 934 was observed. The evolution of the Cu2p XPS spectra clearly shown oxidation from Cu^+ to a mixture of Cu^+ and Cu^{+2}[53].

The photocalytic activities of the Cu_2Se-graphene nanocomposite using Rh.B as organic dye under visible irradiation was investigated and shown in Figure 6 (a-f). The decline intensity of electronic absorption spectra demonstrates the degradation of Rh.B in the presence of Cu_2Se-graphene catalysts. In the degradation process two essential steps are involved (1) the absorption by the photocatalyst and (2) the fast charge transfer route; these two steps are one kind of reason of the decomposition for the organic pollutants. In this study, the gra-

phene is acts as an adsorption support material and dye molecules absorbed on the surface of graphene via π-π interaction. The Figure 6 (a-c) clearly indicates that the concentration of Rh.B with the different interval of time changed, which shows the adsorption and electron charge transfer ability of the Cu_2Se-graphene nanocomposites. For achieving adsorption-desorption equilibrium, the prepared sample was kept in dark for 2 h, after obtain the adsorption-desorption equilibrium, the solution was kept in closed box and turn on visible light. From the Figure 6 (a-c), it shows the photocatalytic performance of the Cu_2Se-graphene nanocomposites in term of photo degradation of Rh.B molecules under visible light irradiation. During the increasing of the irradiation time, the intensity of the characteristic absorption band of Rh.B (554 nm) was significantly decreased. The concentration changes of Rh.B solution were recorded and Figure 6 (c-d) clearly shows that approximately 95% of the organic dye was degraded by Cu_2Se-graphen-3 nanocomposite after 180 min as irradiation time. The kinetics of the degradation can be expressed by using the Langmuir-Hinshelwood model, can be expressed as $-\ln(C_t/C_o) = K_{app}t$, where, $K_{app}t$ is apparent rate constant, and C_O initial concentration at $t = 0$ and C_t are the concentration of dye at $t = t$[54]. The kinetic plot and apparent rate constant (K_{aap}) of the Cu_2Se-graphene-3 were shown in Figure 6 (e). It can be clearly seen that Cu_2Se-graphene-3 catalyst exhibited highest visible light activity ($K_{app} = 5.32 \times 10^{-3}$ min^{-1}), indicating that the Cu_2Se-graphene-3 is highly effective catalytic materials for photodegradation. Besides the excellent photocatalytic efficiency , the stability of the catalytic is also essential to the application of a photocatalyst[55]. To investigating the stability and reusability of the Cu_2Se-graphene composites, the cyclic runs in the photocatalyitc degradation of Rh.B in the presence of Cu_2Se-graphene under visible light are also studied. Figure 5(f) shows that Cu_2Se-graphene minor decrease first two cycles of the photodegradation of Rh. B. The decomposition rates for 1^{st} 2^{nd} 3^{rd} and 4^{th} cycles were 18.62, 18.10, 16.23 and 12.33% respectively. And, the results concluded that the Cu_2Se-graphene composites have moderate stability. It seems like a promising candidate for environmental sanctification.

4. Conclusion

Cu_2Se-graphene has been prepared via microwave-assisted technique. SEM and TEM images clearly show that Cu_2Se was unevenly distributed onto the surface of the graphene sheets. The details revealed that Cu_2Se-grapheen is effective catalyst for photodegradation. Moreover, the cyclic reusability explained that Cu_2Se-graphene nanocomposites are a favorable candidate for environmental mediation. In this study, it presented that graphene is one kind of candidate as based material to develop remarkably efficient binary system for photocatalytic degradation of organic dyes.

References

1. H. Kyung, J. Lee, and W. Choi, Simultaneous and synergistic conversion of dyes and heavy metal ions in aqueous TiO_2 suspensions under visible-light illumination, *Environ. Sci. Technol.*, **39**(7), 2376-2382 (2005).
2. R. Vinu and G. Madras, Photocatalytic activity of Ag-substituted and impregnated nano-TiO_2, *Appl. Catal. A*, **366**(1), 130-140 (2009).
3. A. R. Ghadim, S. Aber, A. Olad, and H. ASorkhabi, Optimization of electrocoagulation process for removal of an azo dye using response surface methodology and investigation on the occurrence of destructive side reactions, *Chem. Eng. Process.*, **64**, 68-78 (2013).
4. M. Anas, D. S. Han, K. Mahmoud, H. Park, and A. A. Wahab, Photocatalytic degradation of organic dye using titanium dioxide modified with metal and non-metal deposition, *Mater. Sci. Semicond. Process.*, **41**, 209-218 (2016).
5. H. P. Carvalho, J. Huang, M. Zhao, G. Liu, L. Dong, and X. Liu, Improvement of Methylene Blue removal by electrocoagulation/banana peel adsorption coupling in a batch system, *Alex. Eng. J.*, **54**(3), 777-786 (2015).
6. G. G. Bessegato, J. C. Cardoso, B. F. da Silva, and M. V. Boldrin Zanoni, Combination of photoelectrocatalysis and ozonation: A novel and powerful approach applied in Acid Yellow 1 mineralization, *Appl. Catal. B*, **180**, 161-168 (2016).
7. B. M. Esteves, C. D Rodrigues, R. Boaventura, F. M. Hódar, and L. M. Madeira, Coupling of acrylic dyeing wastewater treatment by heterogeneous Fenton oxidation in a continuous stirred tank reactor with biological degradation in a sequential batch reactor, *J. Environ. Manag.*, **166**, 193-203 (2016).
8. K. Shakir, A. F. Elkafrawy, H. F. Ghoneimy, S. G. Beheir, and M. Refaat, Removal of rhodamine B (a basic dye) and thoron (an acidic dye) from dilute aqueous solutions and wastewater simulants by ion flotation, *Water Res.*, **44**(5), 1449-1461 (2010).
9. Z. D. Meng and W. C. Oh, Sonocatalytic degradation and catalytic activities for MB solution of Fe treated fullerene/TiO_2 composite with different ultrasonic intensity, *Ultrason. Sonochem.*, **18**(3), 757-764 (2011).
10. M. Sun, Y. Fang, Y. Wang, S. Sun, J. He, and Z. Yan, Synthesis of Cu_2O/graphene/rutile TiO_2 nanorod ternary composites with enhanced photocatalytic activity, *J. Alloys Compd.*, **650**, 520-527 (2015).
11. Y. Leng, Y. Gao, W. Wang, and Y. Zhao, Continuous supercritical solvothermal synthesis of TiO_2-pristine-graphene hybrid as the enhanced photocatalyst, *J. Supercrit. Fluids*, **103**, 115-121 (2015).
12. M. A Rauf and S. S. Ashraf, Fundamental principles and application of heterogeneous photocatalytic degradation of dyes in solution, *Chem. Eng. J.*, **151**(1), 10-18 (2009).
13. A. Senthilraja, B. Subash, B. Krishnakumar, D. Rajamanickam, M. Swaminathan, and M. Shanthi, Synthesis, characterization and catalytic activity of co-doped Ag-Au-ZnO for MB dye degradation under UV-A light, *Mater. Sci. Semicond. Process.*, **22**, 83-91 (2014).
14. S. Rtimi, C. Pulgarin, R. Sanjines, and J. Kiwi, Kinetics and mechanism for transparent polyethylene-TiO_2 films mediated self-cleaning leading to MB dye discoloration under sunlight irradiation, *Appl. Catal. B*, **162**, 236-244 (2015).
15. N. D. Phu, L. H. Hoang, X. Chen, M. Hong Kong, H. C. Wen, and W. C. Chou, Study of photocatalytic activities of Bi_2WO_6 nanoparticles synthesized by fast microwave-assisted method, *J. Alloys Compd.*, **647**, 123-128 (2015).
16. J. Zhang, L. J. Xu, Z. Q. Zhu, and Q. J. Liu, Synthesis and properties of (Yb, N)-TiO_2 photocatalyst for degradation of methylene

blue (MB) under visible light irradiation, *Mater. Res. Bull.*, **70**, 358-364 (2015).
17. Y. Sha, I. Mathew, Q. Cui, M. Clay, F. Gao, X. J. Zhang, and Z. Gu, Rapid degradation of azo dye methyl orange using hollow cobalt nanoparticles, *Chemosphere*, **144**, 1530-1535 (2016).
18. Y. Cao, X. Gu, H. Yu, W. Zeng, Xi. Liu, S. Jiang, and Y. Li, Degradation of organic dyes by Si/SiO_x core-shell nanowires: Spontaneous generation of superoxides without light irradiation, *Chemosphere*, **144**, 836-841 (2016).
19. D. Das and R. K. Dutta, A novel method of synthesis of small band gap SnS nanorods and its efficient photocatalytic dye degradation, *J. Colloid Interface Sci.*, **457**, 339-344 (2015).
20. N. K. R. Bogireddy, H. A. K. Kumar, and B. K. Mandal, Biofabricated silver nanoparticles as green catalyst in the degradation of different textile dyes, *J. Environ. Chem. Eng.*, **4**(1), 56-64 (2016).
21. K. Mahesh and D. H. Kuo, Synthesis of Ni nanoparticles decorated SiO_2/TiO_2 magnetic spheres for enhanced photocatalytic activity towards the degradation of azo dye, *Appl. Surf. Sci.*, **357**, 433-438 (2015).
22. A. Jagminas, R. Juškėnas, I. Gailiūtė, G. Statkutė, and R. Tomašiūnas, Electrochemical synthesis and optical characterization of copper selenide nanowire arrays within the alumina pores, *J. Cryst. Growth*, **294**(2), 343-348 (2006).
23. T. D. T. Ung and Q. L. Nguyen, Synthesis, structural and photocatalytic characteristics of nano-$Cu_{2-x}Se$, *Adv. Nat. Sci.: Nanosci. Nanotechnol.*, **2**(4), 045003 (2011).
24. M. J. Allen, V. C. Tung, and R. B. Kaner, Honeycomb carbon: a review of graphene, *Chem. Rev.*, **110**(1), 132-145 (2009).
25. A. Konstantin Geim, Graphene: status and prospects, *Science*, **324**(5934), 1530-1534 (2009).
26. Y.-K. Seo, G. Hundal, I. T. Jang, Y. K. Hwang, C.-H. Jun, and J.-S. Chang, Microwave synthesis of hybrid inorganic-organic materials including porous $Cu_3(BTC)_2$ from Cu(II)-trimesate mixture Microporous, *Mesoporous Mater.*, **119**, 331-337 (2009).
27. K. M. L. Taylor-Pashow, J. D. Rocca, Z. Xie, S. Tran, and W. Lin, Postsynthetic modifications of iron-carboxylate nanoscale metal-organic frameworks for imaging and drug delivery, *J. Am. Chem. Soc*., **131**, 14261-14263 (2009).
28. N. A. Khan and S. H. Jhung, Synthesis of metal-organic frameworks (MOFs) with microwave or ultrasound: Rapid reaction, phase-selectivity, and size reduction, *Coord. Chem. Rev.*, **285**, 11-23 (2015).
29. J. S. Choi, W. J. Son, J. Kim, and W.-S. Ahn, Metal-organic framework MOF-5 prepared by microwave heating: factors to be considered, *Microporous Mesoporous Mater.*, **116**, 727-731 (2008).
30. W. L. Liu, L. H. Ye, X. F. Liu, L. M. Yuan, X. L. Lu, and J. X. Jiang, Rapid synthesis of a novel cadmium imidazole-4, 5-dicarboxylate metal-organic framework under microwave-assisted solvothermal condition, *Inorg. Chem. Commun*, **11**, 1250-1252 (2008).
31. I. Bilecka and M. Niederberger, Microwave chemistry for inorganic nanomaterials synthesis, *Nanoscale*, **2**, 1358-1374 (2010).
32. K. J. Rao, B. Vaidhyanathan, M. Ganguli, and P. A. Ramakrishnan, Synthesis of inorganic solids using microwaves, *Chem. Mater.*, **11**(4), 882-895 (1999).
33. M. Rajamathi and R. Seshadri, Curr. Opin, Oxide and chalcogenide nanoparticles from hydrothermal/solvothermal reactions, *Solid State Mater. Sci.*, **6**, 337-345 (2002).
34. S. Komarneni, Nanophase materials by hydrothermal, microwave-hydrothermal and microwave-solvothermal methods, *Curr. Sci*., **85**(12), 1730-1734 (2003).
35. S. Z. Shi and J.-Y. Hwang, Microwave-assisted wet chemical synthesis: Advantages, significance, and steps to industrialization, *J. Miner. Mater. Charact. Eng.*, **2**, 101-110 (2003).
36. K. Ullah, A. Ali, S. Ye, L. Zhu, and W. C. Oh, Microwave- assisted synthesis of Pt-graphene/TiO_2 nanocomposites and their efficiency in assisting hydrogen evolution from water in the presence of sacrificial agents, *Sci. Adv. Mater.,* **7**(4), 606-614 (2015).
37. W. C. Oh and F. J. Zhang, Preparation and characterization of graphene oxide reduced from a mild chemical method, *Asian J. Chem.*, **23**(2), 875-879 (2011).
38. M. L. Chen, C. Y. Park, J. G. Choi, and W. C. Oh, Synthesis of characterization of metal (Pt, Pd and Fe)-graphene composites, *J. Korean. Ceram. Soc.*, **48**(2), 147-151 (2011).
39. H. Liu, X. Shi, F. Xu, L. Zhang, W. Zhang, L. Chen, Q. Li, C. Uher, T. Day, and G .Jeffrey Snyder, Copper ion liquid-like thermoelectrics, *Nat. Mater.*, **11**(5), 422-425 (2012).
40. V. M. Glazov, A. S. Pashinkin, and V. A. Fedorov, Phase equilibria in the Cu-Se system, *Inorg. Mater.*, **36**(7), 641-652 (2000).
41. S. D. Perera, R. G. Mariano, K. Vu, N. Nour, O. Seitz, Y. Chabal, and K. J. Balkus Jr, Hydrothermal synthesis of graphene-TiO_2 nanotube composites with enhanced photocatalytic activity, *ACS Catal.*, **2**(6), 949-956 (2012).
42. B. Pejova, Optical phonons in nanostructured thin films composed by zincblende zinc selenide quantum dots in strong size-quantization regime: Competition between phonon confinement and strain-related effects, *J. Solid State Chem.*, **213**, 22-31 (2014).
43. L. M. Malard, M. A. Pimenta, G. Dresselhaus, and M. S. Dresselhaus, Raman spectroscopy in graphene, *Phys. Rep.*, **473**(5), 51-87 (2009).
44. Q. Xiang, J. Yu, and M. Jaroniec, Synergetic effect of MoS_2 and graphene as cocatalysts for enhanced photocatalytic H_2 production activity of TiO_2 nanoparticles, *J. Am. Chem. Soc.*, **134**(15), 6575-6578 (2012).
45. B. Tang, H. Guoxin, and H. Gao, Raman spectroscopic characterization of graphene, *Appl. Spectrosc. Rev.*, **45**(5), 369-407 (2010).
46. T. Ghosh, K. Ullah, V. Nikam, C. Y. Park, Z. D. Meng, and W. C. Oh, The characteristic study and sonocatalytic performance of CdSe-graphene as catalyst in the degradation of azo dyes in aqueous solution under dark conditions, *Ultrason. Sonochem.*, **20**(2), 768-776 (2013).
47. K. N. Kudin, B. Ozbas, H. C. Schniepp, R. K. Prud'Homme, I. A. Aksay, and R. Car, Raman spectra of graphite oxide and functionalized graphene sheets, *Nano Lett.*, **8**(1), 36-41 (2008).
48. S. C. Riha, D. C. Johnson, and A. L. Prieto, Cu_2Se nanoparticles with tunable electronic properties due to a controlled solid-state phase transition driven by copper oxidation and cationic conduction, *J. Am. Chem. Soc.*, **133**(5), 1383-1390 (2010).
49. W. Fan, Q. Zhang, and Y. Wang Semiconductor-based nanocomposites for photocatalytic H_2 production and CO_2 conversion, *Phys. Chem. Chem. Phys.*, **15**, 2632-2649 (2013).
50. T. Szabo, O. Berkesi, P. Forgó, K. Josepovits, Y. Sanakis, D. I, Petridis, and I. Dékány, Evolution of surface functional groups in a series of progressively oxidized graphite oxides, *Chem. Mater*., **18**, 2740-2749 (2006).

51. H. K. Jeong, H. J. Noh, J. Y, Kim, M. H. Jin, C. Y. Park, and Y. H. Lee, X-ray absorption spectroscopy of graphite oxide, *Europhys. Lett.*, **82**, 67004-67005 (2008).
52. X. Chen, S. Shen, L. Guo, and S. Mao, Semiconductor-based Photocatalytic Hydrogen Generation, *Chem. Rev*., **210**, 6503-6570 (2010).
53. D. Cahen, P. J. Ireland, L. L. Kazmerski, and F. A. Thiel, X-ray photoelectron and Auger electron spectroscopic analysis of surface treatments and electrochemical decomposition of $CuInSe_2$ photoelectrodes, *J. Appl. Phys.*, **5**, 4761-4771 (1985).
54. J. Kyriakopoulos, M. D. Tzirakis, G. D. Panagiotou, M. N. Alberti, K. S. Triantafyllidis, S. Giannakaki, K. Bourikas, C. Kordulis, M. Orfanopoulos, and A. Lycourghiotis, Highly active catalysts for the photooxidation of organic compounds by deposition of [60] fullerene onto the MCM-41 surface: A green approach for the synthesis of fine chemicals, *Appl. Chem. B*, **117**, 36-48 (2012).
55. Y. Wang, R. Shi, J. Lin, and Y. Zhu, Enhancement of photocurrent and photocatalytic activity of ZnO hybridized with graphite-like C_3N_4, *Energy Environ. Sci.*, **4**(8), 2922-2929 (2011).